IEEE Robotics and Automation Letters (RA-L) paper, presented at ICRA 2026, Vienna, Austria. Cite as RA-L paper.

Harmonising Safety Paradigms: Energy-Aware Control of Active Response and Passive Compliance for Safety-Critical Robotic Tasks

Xinyuan Zhao[1], Wenyu Liang[1], Junyuan Xue[1,2], and Yan Wu[1]

***Abstract*—Ensuring safety in robotic manipulation is increasingly critical as robots become integrated into human-shared environments for complex physical interaction tasks. This paper presents an energy-aware control framework that combines active responses with passive compliance for safety-critical robotic manipulation. Specifically, Control Barrier Functions (CBFs) are employed for active collision avoidance with detected obstacles, which are then integrated with fallback safety actions to resolve potential violation of CBF constraints. Complementing this active safety paradigm, a passive safety paradigm is implemented to mitigate post-collision impacts by monitoring energy variance and limiting power exchanges. Furthermore, an energy tank is incorporated to enforce passivity of the robot, which is crucial to address potential instability issues in variable impedance control. To make the tank adaptive to varying energy requirements arising from dynamic environments and unpredictable events, we propose a novel, task-agnostic tank recharging condition without compromising the system's passivity guarantee. The effectiveness of the proposed control framework is validated through experiments on a KUKA iiwa 14 robot.**

***Index Terms*—Safety in HRI, Motion Control, Compliance and Impedance Control**

I. Introduction

THE integration of robots into human-shared environments has rapidly advanced recently, emphasizing the urgent need to ensure operational safety. Particularly for robotic manipulators performing collaborative tasks in proximity to humans, they must not only accomplish nominal objectives (e.g., trajectory tracking or force regulation) but also guarantee robust safety in the presence of dynamic obstacles, uncertain perceptions, and direct physical interactions with humans.

Control Barrier Functions (CBFs) have emerged as a popular active-safety paradigm, offering formal guarantees that system states always remain within predefined safe sets [1], [2]. By embedding CBFs into quadratic programming (QP) formulations, real-time generation of safety-guaranteed trajectories has been demonstrated across diverse robots [3]–[7]. However, CBF constraints may not always be satisfiable, particularly when dealing with dynamic obstacles or in the presence of perception noise, which raises the critical question of how to address safety challenges when CBF constraints are violated. Furthermore, CBFs are typically for maintaining predefined safe states such as keeping distances from obstacles or avoiding singularities in configuration space. They are inherently not for complex and unpredictable dynamics involved in physical interactions, which, however, is unavoidable in human-robot collaboration scenarios.

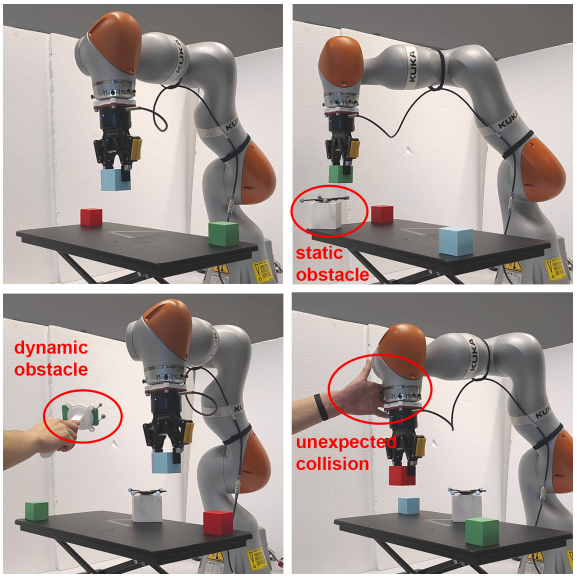

Fig. 1: A KUKA iiwa 14 robot for pick-and-place tasks while dealing with different safety issues. Top Left: The normal case of pick-and-place tasks. Top Right: The robot avoids collision with a static obstacle. Bottom Left: The robot avoids collision with a dynamic obstacle. Bottom Right: The robot mitigates unexpected collision via compliant reactions.

On the other hand, variable impedance control (VIC) has been widely explored to generate physical interactions with humans and unknown environments. By modulating the impedance parameters dynamically, a balance can be achieved between precise execution of the given tasks and compliant responses to disturbances. However, it is known in the literature [8] that variable impedance control may introduce unstable behaviors due to energy injection and the violation of passivity. This can be addressed by leveraging energy tank techniques [9]–[14], which formally restore passivity of the integrated system by imposing bounded energy budgets for performing non-passive actions.

While effective, it remains an open problem to set a proper energy budget that is robust to inaccurate dynamics (like frictions) and varying energy requirements arising from, e.g., collision avoidance, human interaction and other unpredictable events in human-robot collaboration scenarios. Energy budgets are typically estimated from nominal task execution and thus may terminate the task prematurely when unexpected energy

This work was supported by the National Robotics Programme BAU Grant M23NBK0053, Singapore.

[1] Institute for Infocomm Research (I^{2}R), Agency for Science, Technology and Research (A*STAR), Singapore. {zhao_xinyuan, liang_wenyu, wuy}@a-star.edu.sg

[2] Department of Electrical and Computer Engineering, National University of Singapore, Singapore. xue.junyuan@u.nus.edu

©2026 IEEE

demands occur. Nevertheless, an overly large energy budget might not provide sufficient constraints to prevent the aforementioned instability issues [15]. A solution is to incorporate a tank supervisor [8] for dynamic energy allocation. Recent advancements in this direction suggest assigning energy budgets at each control loop, either relying on pre-optimized nominal motions [16], [17] or reinforcement learning (RL) agents trained on specific tasks [18]. However, these approaches lack adaptability to varying energy demands, thus unsuitable for safety-critical applications where safety challenges can be diverse and unpredictable. Moreover, as noted in the literature [17], [19], dynamic recharging operations would compromise the passivity guarantees provided by energy tanks, potentially bringing back the instability issues.

While existing works have attempted to integrate complementary safety mechanisms and passivity guarantees, some limitations remain. For instance, [20], [21] proposed frameworks that aim at achieving integrated active and passive safety mechanisms. However, [20] employs energy tanks without dynamic recharging, while [21] achieves only conditional passivity through relaxation. Furthermore, neither provides an explicit fallback action for CBF constraint failures. Regarding dynamic recharging for energy tanks, the approaches presented by [17], [18] are not well-suited for scenarios with time-varying energy demands. Moreover, these works only explore passive safety mechanisms, neglecting active responses to safety challenges.

Motivated by these observations, we propose a control framework for safety-critical robotic manipulation that systematically integrates active and passive safety mechanisms while preserving the system's passivity through flexible, task-agnostic energy management. It aims to handle diverse safety challenges encountered in human-shared environments, from avoiding dynamic obstacles to managing unexpected collisions, all while ensuring successful task completion.

The main contributions of this paper are summarized below. Firstly, a control framework integrating both active and passive safety paradigms is proposed for safety-critical robotic manipulation. The active paradigm utilizes CBFs for obstacle avoidance, augmented with fallback action for robustness against moving obstacles and perception noise, while the passive paradigm implements post-impact mitigation for unavoidable collision or unexpected interaction.

Secondly, an energy tank is incorporated to enforce passivity, accompanied by a novel condition for dynamic tank recharging. The recharging condition is task-agnostic, robust to disturbances and dynamic environments while minimizing violation of the formal passivity, rendering the system *almost-everywhere-passive*. To the best of our knowledge, this is the first time of proposing such a tank recharging condition that is particularly suitable for dynamic environments like human-robot collaboration scenarios.

Lastly, hardware experiments are conducted to validate the proposed framework. These experiments demonstrate the effectiveness of using the energy tank with our recharging condition in maintaining system stability under variable impedance control. It also shows the integrated framework's capability to successfully handle various safety challenges within a practical pick-and-place task as illustrated in Fig. 1.

II. Preliminary

A. Control Barrier Functions

CBFs have emerged as a powerful tool for ensuring the safety of robotic systems by mathematically defining a safe set and synthesizing control laws that guarantee the system remains within the boundaries. For a system with state $z \in \mathcal{D} \subset \mathcal{R}^n$ and input $u \in \mathcal{U} \subset \mathcal{R}^m$, a safe set $\mathcal{S}$ defined as the 0-super-level set of a continuously differentiable function $h : \mathcal{D} \mapsto \mathbb{R}$ can be introduced as:

$$\mathcal{S} := \{z \in \mathcal{D} \subset \mathcal{R}^n : h(z) \geq 0\}, \tag{1}$$

such that the system is safe if z always stays within $\mathcal{S}$. The forward invariance of $\mathcal{S}$ can be achieved if there exists an extended class $\mathcal{K}$ function $\alpha : \mathbb{R} \mapsto \mathbb{R}$ such that

$$\sup_{u \in \mathcal{U}} \dot{h}(z) \geq -\alpha(h(z)), \quad \forall z \in \mathcal{D}. \tag{2}$$

Under such circumstances, the function h is also known to be a CBF [2]. Given a CBF, there is an associated safe control set

$$\mathcal{K}_{\text{cbf}}(z) = \{u \in \mathcal{U} : \dot{h}(z) \geq -\alpha(h(z))\}, \tag{3}$$

which defines the control inputs that render the safe set $\mathcal{S}$ to be forward invariant and thus ensure the system's safety.

B. Cartesian Impedance Control

The dynamics of a fully-actuated robot with n joints can be modeled as follows in the Cartesian space [22], [23]

$$\boldsymbol{\Lambda}(\boldsymbol{x})\ddot{\boldsymbol{x}} + \boldsymbol{\mu}(\boldsymbol{x}, \dot{\boldsymbol{x}})\dot{\boldsymbol{x}} = \boldsymbol{J}(\boldsymbol{q})^{-\mathrm{T}}\boldsymbol{\tau} + \underbrace{\boldsymbol{J}(\boldsymbol{q})^{-\mathrm{T}}\boldsymbol{\tau}_{\mathrm{e}}}_{\boldsymbol{F}_{\mathrm{e}}}, \tag{4}$$

where $\boldsymbol{q}$ denotes the joint configurations and $\boldsymbol{x}$ denotes the Cartesian pose of the end-effector (EE). $\boldsymbol{\Lambda}(\boldsymbol{x})$ and $\boldsymbol{\mu}(\boldsymbol{x}, \dot{\boldsymbol{x}})$ denote the inertia matrix and Coriolis matrix, respectively, and $\boldsymbol{J}(\boldsymbol{q})$ denotes the Jacobian matrix such that $\dot{\boldsymbol{x}} = \boldsymbol{J}(\boldsymbol{q})\dot{\boldsymbol{q}}$. $\boldsymbol{\tau}$ denotes the actuation torques, and $\boldsymbol{\tau}_{\mathrm{e}}$ denotes the torques induced by external disturbances or interactions. Without loss of generality, we follow a common assumption that the gravitational effect has been compensated and thus vanishes from the dynamics.

Cartesian impedance control aims to achieve a desired relationship between the EE's motion and external interactions [24]. Specifically, defining the error $\tilde{\boldsymbol{x}} = \boldsymbol{x} - \boldsymbol{x}_{\mathrm{d}}$ between $\boldsymbol{x}$ and the desired position $\boldsymbol{x}_{\mathrm{d}}$, the control objective is to achieve a closed-loop dynamics of the form [23]

$$\boldsymbol{\Lambda}\ddot{\tilde{\boldsymbol{x}}} + (\boldsymbol{\mu} + \boldsymbol{D}_{\mathrm{d}})\,\dot{\tilde{\boldsymbol{x}}} + \boldsymbol{K}_{\mathrm{d}}\tilde{\boldsymbol{x}} = \boldsymbol{F}_{\mathrm{e}}, \tag{5}$$

where $\boldsymbol{K}_{\mathrm{d}}$ and $\boldsymbol{D}_{\mathrm{d}}$ are the symmetric and positive definite matrices of desired stiffness and damping, respectively. Then the Cartesian impedance control (5) can be implemented by controlling torques in the following form

$$\boldsymbol{\tau} = \boldsymbol{J}^{\mathrm{T}}\left(\boldsymbol{\Lambda}\ddot{\boldsymbol{x}}_{\mathrm{d}} + \boldsymbol{\mu}\dot{\boldsymbol{x}} - \boldsymbol{K}_{\mathrm{d}}\tilde{\boldsymbol{x}} - \boldsymbol{D}_{\mathrm{d}}\dot{\tilde{\boldsymbol{x}}}\right). \tag{6}$$

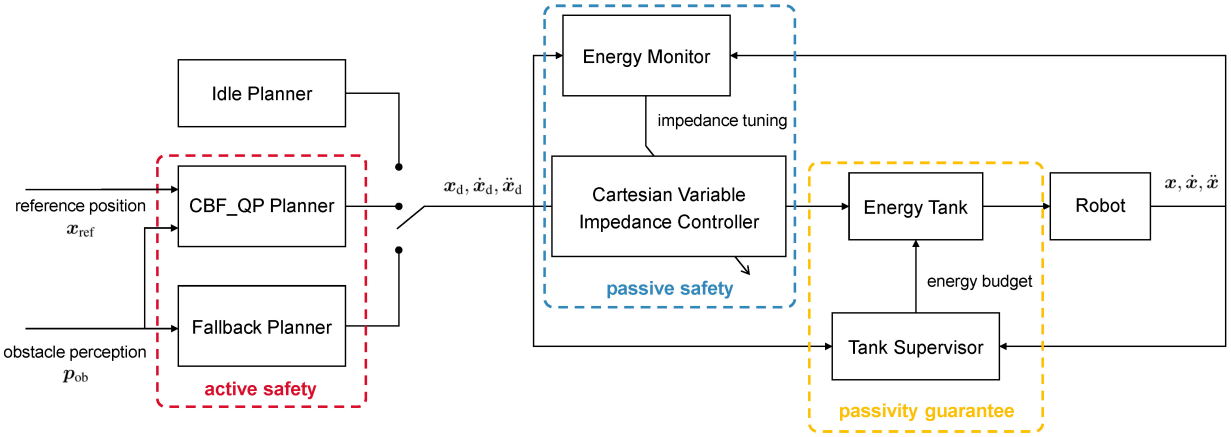

Fig. 2: Diagram of the proposed control framework. It consists of three core modules: an active safety module, a passive safety module, and a passivity guarantee module.

C. Passivity and Energy Tank

For conventional impedance control where the stiffness and damping are constant during operation, it has been proved that the robot is essentially stable [23]. However, when impedance parameters are designed to be variable, the essential stability is no longer guaranteed [8], [9]. From the perspective of energy, loosely speaking, the system under variable impedance control can generate unbounded energy automatically, violating the condition of passivity and thus jeopardizing its stability.

Energy tanks have been introduced in the energy-aware framework [8] and are used to recover passivity of control systems whenever non-passive actions need to be implemented. To be specific, an energy tank is a virtual energy storage system in the form of [17], [18]

$$\begin{cases} \dot{x}_\mathrm{t}(t) = u_\mathrm{t}(t) \\ y_\mathrm{t}(t) = \frac{\partial T}{\partial x_\mathrm{t}} = x_\mathrm{t}(t), \end{cases} \tag{7}$$

where $x_\mathrm{t} \in \mathbb{R}$ denotes the state of the tank and $u_\mathrm{t}, y_\mathrm{t} \in \mathbb{R}$ denote the input and output port variables of the tank, respectively. The energy stored in the tank can then be represented by a non-negative function $T(x_\mathrm{t})$ as

$$T(x_\mathrm{t}) = \frac{1}{2} x_\mathrm{t}^2 \tag{8}$$

Combining (7) and (8) yields

$$\dot{T}(x_\mathrm{t}) = u_\mathrm{t}(t) y_\mathrm{t}(t). \tag{9}$$

For instance, to reproduce desired actions $\boldsymbol{\tau}_\mathrm{d}$, including those that are non-passive, to the system (4) while maintaining its passivity, the energy tank can be interconnected in a power-preserving way as follows

$$\begin{bmatrix} \boldsymbol{\tau} \\ u_\mathrm{t} \end{bmatrix} = \begin{bmatrix} \mathbf{0} & -\boldsymbol{a} \\ \boldsymbol{a}^\mathrm{T} & 0 \end{bmatrix} \begin{bmatrix} \dot{\boldsymbol{q}} \\ y_\mathrm{t} \end{bmatrix}, \tag{10}$$

where $\boldsymbol{a}(t) = -\frac{\boldsymbol{\tau}_\mathrm{d}(t)}{x_\mathrm{t}(t)}$ represents a transformation ratio modulated by the tank state x_t. Combining (9) and (10) yields

$$\dot{T}(x_\mathrm{t}) = u_\mathrm{t}(t) y_\mathrm{t}(t) = -\dot{\boldsymbol{q}}^\mathrm{T}(t) \boldsymbol{\tau}(t). \tag{11}$$

where the inner product $\dot{\boldsymbol{q}}^\mathrm{T}\boldsymbol{\tau}$ represents the instantaneous power injected into the robot by the actuators. (11) reveals that the power flowing through the port $(u_\mathrm{t}, y_\mathrm{t})$ of the tank is the same as the power flowing through the port $(\boldsymbol{\tau}, \dot{\boldsymbol{q}})$ of the robot, consequently proving the interconnection (10) is indeed *power-preserving*. Additionally, combining (7) and (10) provides

$$\boldsymbol{\tau}(t) = -\boldsymbol{a}(t) y_\mathrm{t}(t) = \boldsymbol{\tau}_\mathrm{d}(t), \tag{12}$$

which implies the reproduction of the desired action $\boldsymbol{\tau}_\mathrm{d}$. Nevertheless, when the tank depletes, the control actions have to be scaled accordingly to keep the closed-loop system always passive.

III. Methodology

This section presents the proposed framework for safety-critical robotic manipulation, illustrated in Fig. 2. The framework consists of three core modules: an active safety module, a passive safety module, and a passivity guarantee module. For disambiguation, *passive safety* refers to an operational mode that exploits mechanical compliance for post-impact mitigation during physical interactions, whereas *passivity* denotes a theoretical property that prevents a system from generating net energy on its own, thus crucial for stability.

A. Active Safety Paradigm

To generate active avoidance of obstacles while performing the desired task, a QP problem is formulated as follows with a double-integrator model describing the EE's motion and the CBF constraints (2) naturally integrated

$$\min_{[\boldsymbol{x}_\mathrm{d}, \dot{\boldsymbol{x}}_\mathrm{d}, \ddot{\boldsymbol{x}}_\mathrm{d}]} \beta_a \|\boldsymbol{x}_\mathrm{d} - \boldsymbol{x}_\mathrm{ref}\|_2^2 + \beta_b \|\dot{\boldsymbol{x}}_\mathrm{d}\|_2^2 + \beta_c \|\ddot{\boldsymbol{x}}_\mathrm{d}\|_2^2 \tag{13}$$

$$\text{s.t.} \ \frac{\mathrm{d}}{\mathrm{d}t} \begin{bmatrix} \boldsymbol{x}_\mathrm{d} \\ \dot{\boldsymbol{x}}_\mathrm{d} \end{bmatrix} = \begin{bmatrix} \mathbf{0} & \boldsymbol{I} \\ \mathbf{0} & \mathbf{0} \end{bmatrix} \begin{bmatrix} \boldsymbol{x}_\mathrm{d} \\ \dot{\boldsymbol{x}}_\mathrm{d} \end{bmatrix} + \begin{bmatrix} \mathbf{0} \\ \boldsymbol{I} \end{bmatrix} \ddot{\boldsymbol{x}}_\mathrm{d} \tag{13a}$$

$$\boldsymbol{v}_\mathrm{low} \le \dot{\boldsymbol{x}}_\mathrm{d} \le \boldsymbol{v}_\mathrm{up} \tag{13b}$$

$$\boldsymbol{a}_\mathrm{low} \le \ddot{\boldsymbol{x}}_\mathrm{d} \le \boldsymbol{a}_\mathrm{up} \tag{13c}$$

$$\dot{h}_i(\boldsymbol{x}_\mathrm{d}, \boldsymbol{p}_{\mathrm{ob},i}) \ge -\alpha_i(h_i(\boldsymbol{x}_\mathrm{d}, \boldsymbol{p}_{\mathrm{ob},i})) \tag{13d}$$

$$h_i(\boldsymbol{x}_\mathrm{d}, \boldsymbol{p}_{\mathrm{ob},i}) \ge 0 \tag{13e}$$

where $\boldsymbol{x}_\mathrm{d}$, $\dot{\boldsymbol{x}}_\mathrm{d}$ and $\ddot{\boldsymbol{x}}_\mathrm{d}$ represent the desired trajectory to track by the Cartesian impedance controller. $\boldsymbol{x}_\mathrm{ref}$ is the reference waypoint given by the task. $\boldsymbol{v}_\mathrm{low}$, $\boldsymbol{v}_\mathrm{up}$, $\boldsymbol{a}_\mathrm{low}$ and $\boldsymbol{a}_\mathrm{up}$ denote

the lower and upper bounds for velocities and accelerations, respectively. $\boldsymbol{p}_{\text{ob},i}$ represents the position of the i-th obstacle. For each obstacle, the CBF is designed to be

$$h_i(\boldsymbol{x}_\text{d}, \boldsymbol{p}_{\text{ob},i}) = \|\boldsymbol{x}_\text{d} - \boldsymbol{p}_{\text{ob},i}\|_2^2 - r_i^2, \tag{14}$$

where r_i represents the safety margin for the i-th obstacle. The function $\alpha_i(\cdot)$ is designed to be an identity function, i.e., $\alpha_i(h_i) = h_i$.

Notably, the CBF constraint (13d) regulates the relationship between $h_i(\cdot)$ and its time derivative. With the CBF specifically defined by (14), the obstacle's velocity, i.e., $\dot{\boldsymbol{p}}_{\text{ob},i}$ naturally appears in the calculation. This dependency makes the CBF constraint prone to failure in practice, particularly when encountering fast-moving obstacles or perception noise. Rather than relaxing the hard constraints (13d) to maintain feasibility as in previous works [20], [21], [25], we propose a fallback safety action that activates whenever the CBF-QP becomes infeasible. To be specific, when the CBF constraint for the i-th obstacle cannot be satisfied, the robot will attempt to match that obstacle's velocity to maintain safe separation as follows

$$\dot{\boldsymbol{x}}_\text{d} = \text{clamp}\left(\boldsymbol{d}_i \cdot \dot{\boldsymbol{p}}_{\text{ob},i},\ \bar{v}_\text{low},\ \bar{v}_\text{up}\right)\ \boldsymbol{d}_i \tag{15}$$

where $\dot{\boldsymbol{x}}_\text{d}$ represents the desired velocity to track, and $\boldsymbol{d}_i = \frac{\boldsymbol{x} - \boldsymbol{p}_{\text{ob},i}}{\|\boldsymbol{x} - \boldsymbol{p}_{\text{ob},i}\|_2}$ is a unit vector pointing from the i-th obstacle to the EE. Low-pass filtering (smoothing factor $\gamma = 0.1$) is applied to the $\dot{\boldsymbol{x}}_\text{d}$ calculated above to smooth potential discontinuities, and then $\boldsymbol{x}_\text{d}$ is updated accordingly.

By introducing the fallback action, we combine the formal safety guarantees of CBF forward invariance with an intuitive safety strategy when formal methods reach their limits. Additionally, this framework eliminates the restrictive assumption that the safe control set (3) must always be non-empty, which is an assumption frequently violated in practice due to dynamic obstacles and perception uncertainties. This combination enhances the robustness of the active safety paradigm in real-world applications, as our experimental results will demonstrate in Section IV.

Remark 1: The rigorous safety guarantees provided by CBFs rely on strictly enforcing the constraint (2) throughout execution. Thus, either constraint relaxation or fallback actions cannot preserve the rigorous safety guarantees, implying that the robot might collide with obstacles under such control schemes. Moreover, imperfect perception of obstacles due to sensor noise, limited fields of view, or occlusions can also lead to unexpected collisions when applying solely the active safety paradigm.

B. Passive Safety Paradigm

To enhance the active safety alone for comprehensive safety challenges, a passive safety paradigm is augmented to mitigate impacts from unexpected interactions or unavoidable collisions. Common approaches for this purpose mainly include variable impedance control [17], [20] and energy shaping/damping injection [13]. In our framework, we propose to implement an energy monitor for collision detection and adapt impedance parameters for post-collision mitigation.

To be specific, the kinetic and potential energy of a robot (4) under Cartesian impedance control (5) is

$$E = \frac{1}{2}\dot{\boldsymbol{x}}^\text{T}\boldsymbol{\Lambda}\dot{\boldsymbol{x}} + \frac{1}{2}\tilde{\boldsymbol{x}}^\text{T}\boldsymbol{K}_\text{d}\tilde{\boldsymbol{x}}. \tag{16}$$

It should be noted that sudden jumps in E imply external impacts. Also, to obtain reliable and low-latency estimates of E and its derivative (i.e., power) from noisy measurements on hardware, a Kalman filter-based energy monitor is designed as follows

$$\dot{\hat{\boldsymbol{\xi}}} = \begin{bmatrix} 0 & 1 & 0 \\ 0 & 0 & 1 \\ 0 & 0 & 0 \end{bmatrix} \hat{\boldsymbol{\xi}}, \quad o = \begin{bmatrix} 1 & 0 & 0 \end{bmatrix} \hat{\boldsymbol{\xi}}, \tag{17}$$

where $\hat{\boldsymbol{\xi}} = [\hat{E}, \dot{\hat{E}}, \ddot{\hat{E}}]^\text{T}$ represents the filter's state and o represents the filter's observation. The corresponding process and measurement noise covariances are selected as

$$\boldsymbol{Q}_E = \text{diag}\left(10^{-6}, 10^{-6}, 10^{-1}\right), \quad \boldsymbol{R}_E = 10^{-3}. \tag{18}$$

When the estimated power exceeds a predefined threshold, i.e., $|\dot{\hat{E}}| \geq P_\text{limit}$, passive safety mode is triggered by zeroing the stiffness $\boldsymbol{K}_\text{d}$ in the impedance controller (6), which makes the robot fully compliant and consequently minimizes impacts on external objects. In passive safety mode, an idle planner (as shown in Fig. 2) is also implemented to dissipate energy from the robot. The idle planner constantly sets $\dot{\boldsymbol{x}}_\text{d} = \boldsymbol{0}$ and $\ddot{\boldsymbol{x}}_\text{d} = \boldsymbol{0}$, which, by combining (5) and (16), leads to

$$\dot{E} = \dot{\boldsymbol{x}}^\text{T}\boldsymbol{F}_\text{ext} - \dot{\boldsymbol{x}}^\text{T}\boldsymbol{D}_\text{d}\dot{\boldsymbol{x}} \leq \dot{\boldsymbol{x}}^\text{T}\boldsymbol{F}_\text{ext}, \tag{19}$$

because the damping matrix $\boldsymbol{D}_\text{d}$ is positive definite.

Remark 2: The inequality (19) reveals that the robot will keep dissipating energy in passive safety mode. It also implies strict passivity of the robot w.r.t. the external interaction port $(\dot{\boldsymbol{x}}, \boldsymbol{F}_\text{e})$ [19], [26] in passive safety mode without relying on the energy tank.

Remark 3: The threshold P_limit directly corresponds to allowable power exchange, making its selection physically intuitive. For instance, standards such as ISO/TS 15066 [27], [28] provide recommended power/force limits for safe human-robot collaboration.

C. Energy Tank Recharging Strategy

Existing approaches for dynamic tank recharging typically require training or optimization for specific tasks under nominal conditions, which limits their generality across tasks and adaptability to dynamic environments with, e.g., unexpected obstacles and human interaction. Besides, these approaches may technically compromise the passivity guarantee by dynamic recharging operations. To address these limitations, we propose a novel condition for energy tanks recharging which ensures the system remains *almost-everywhere-passive* under recharging operations. Moreover, this is a condition on robot states instead of task specifics, making it task-agnostic and thus well-suited for manipulation tasks involving human interaction and dynamic obstacles.

To be specific, an extended state of the robot is defined as

$$\boldsymbol{s} = \left[\boldsymbol{x}^\text{T}, \dot{\boldsymbol{x}}^\text{T}, \ddot{\boldsymbol{x}}^\text{T}, \boldsymbol{x}_\text{d}^\text{T}, \dot{\boldsymbol{x}}_\text{d}^\text{T}, \ddot{\boldsymbol{x}}_\text{d}^\text{T}\right]^\text{T}, \tag{20}$$

and thus the set $\mathcal{S}_\mathrm{t} = \{\boldsymbol{s}\}$ represents all possible states of the robot during execution. Additionally, another set can be defined as

$$\mathcal{S}_\mathrm{eq} = \{\boldsymbol{s} | \boldsymbol{x} = \boldsymbol{x}_\mathrm{d}, \dot{\boldsymbol{x}} = \boldsymbol{0}, \dot{\boldsymbol{x}}_\mathrm{d} = \boldsymbol{0}\}, \tag{21}$$

which represents equilibrium points where the robot matches the desired state with zero velocity. Subsequently, tank recharging is only permitted when the following condition is satisfied

$$\boldsymbol{s} \in \mathcal{S}_\mathrm{eq}. \tag{22}$$

Notably, $\mathcal{S}_\mathrm{eq}$ is a subset of $\mathcal{S}_\mathrm{t}$ with measure zero. Therefore, the recharging events only occur within a zero-measure set, rendering the closed-loop system *almost-everywhere-passive* during the entire execution. Moreover, combining (16) and the derivation of (19) leads to

$$E = 0, \quad \dot{E} = 0, \quad \forall \boldsymbol{s} \in \mathcal{S}_\mathrm{eq}, \tag{23}$$

which reveals that recharging happens precisely at an energy equilibrium, thereby preventing the recharging operation itself from injecting substantial energy into system, which is crucial for overall operational safety and stability.

Remark 4: The condition (22) restricts tank recharging to some motion equilibrium states. While this may not be suitable for tasks that do not admit static equilibrium, many manipulation tasks naturally incorporate such states in practice. For instance, pick-and-place tasks inherently require static configurations of the robot during grasping and placing. Similarly, assembly, packing, and cleaning tasks involve stationary periods during their execution. Therefore, although the proposed recharging condition may not apply to tasks lacking stationary phases, it shows promise for a broad class of practical manipulation tasks.

Remark 5: The robot will be switched to passive safety mode if the recharging condition is not reached before tank depletion. Energy is only dissipated in this mode (by Eq. (19)), thereby preventing further draining of the tank; meanwhile, the robot responds to physical interactions through passive compliance. Once interaction stops and the robot decelerates to equilibrium, the recharging condition (22) is satisfied, and then the robot switches back to active safety mode to continue predefined tasks. While this behavior may not be preferable in all scenarios, it preserves the passivity guarantee and validity of energy tanks, provides risk negotiation, and enables automatic task resume.

Remark 6: The amount of energy recharged into the tank can be designed adaptively to task requirements and environmental contexts. For instance, one might assign a larger energy budget when confident that the robot is clear of obstacles, while assigning a conservative budget when dynamic obstacles, including humans, are detected in proximity. Such adaptive recharging strategies are under careful investigation and beyond the scope of this paper. For validation purposes, we use a straightforward recharging operation, $T = T_\mathrm{init}$, in our experiments, where T_init denotes the initial budget of the energy tank. Though simple, we believe it is sufficient to demonstrate the flexibility of our recharging condition (22) and its adaptability to dynamic environments.

IV. Experiments and Results

To validate the proposed control scheme, experiments are conducted using a KUKA iiwa 14 robot with torque commands sent via its Fast Robot Interface [29]. The experiments first verify the significance of enforcing passivity for robots under variable impedance control, followed by the validation of our proposed tank recharging strategy. Secondly, a pick-and-place case study is presented to demonstrate the integrated framework's capability to handle diverse safety challenges, including dynamic obstacles and unexpected collisions, while ensuring successful task completion. Ablation studies are also conducted to analyze the effectiveness of each module for overall performance.

To cope with sensor noise and numerical precision in real-world scenarios, we consider the relaxation of $\mathcal{S}_\mathrm{eq}$ in the tank recharging condition (22) by introducing small tolerances $\epsilon_1 = 0.005$ (for position) and $\epsilon_2 = 0.001$ (for velocity) in (21). It is deemed a proper engineering relaxation, which reliably detects equilibrium states and preserves the passivity.

A. Evaluation of Passivity and Tank Recharging

This experiment follows a configuration similar to [9], which was previously validated only in MATLAB simulation with a point-mass model. Our implementation extends this experiment to a hardware robot, aiming to demonstrate the practical issue of instability under variable impedance control and the effectiveness of our solution. Specifically, it requires tracking a periodic trajectory x_d along the y-axis in Cartesian space with time-varying stiffness K_d, that is

$$x_\mathrm{d}(t) = 0.1\sin(t),\ K_\mathrm{d}(t) = 30 + 29\sin(2.45t),\ D_\mathrm{d}(t) = 1.$$

Five comparative trials are conducted:

- **Test-1 (Nominal)**: Standard Cartesian impedance control introduced in Section II.B.
- **Test-2 (Tank)**: Incorporation of a standard energy tank without recharging ($T_\mathrm{init} = 2.0$).
- **Test-3 (Ours)**: Implementation of our proposed tank recharging strategy ($T_\mathrm{init} = 2.0$).
- **Test-4 (Improper Recharging)**: Energy tank with a simple recharging policy that triggers whenever the tank is close to depletion ($T_\mathrm{init} = 2.0$).
- **Test-5 (Excessive Budget)**: Standard energy tank with a large initial budget ($T_\mathrm{init} = 10.0$) without recharging.

Fig. 3 shows video snapshots of Test-1, while Fig. 4 compares the EE's motion along the y-axis for Test-1 and Test-2. The results of Test-1 demonstrate that without passivity guarantees, the robot's motion gradually diverges from the reference trajectory. To protect hardware, we terminate the test when the overshooting magnitude exceeds four times the reference trajectory's magnitude. In contrast, stability has been preserved in Test-2 by incorporating an energy tank to enforce passivity. This comparison highlights the practical significance of maintaining passivity for robots under variable impedance control.

While stability is achieved in Test-2, the task is terminated upon tank depletion. To address this limitation, Test-3 implements the tank recharging condition (22) with results illustrated in Fig. 5. Upon tank depletion, the robot is decelerated

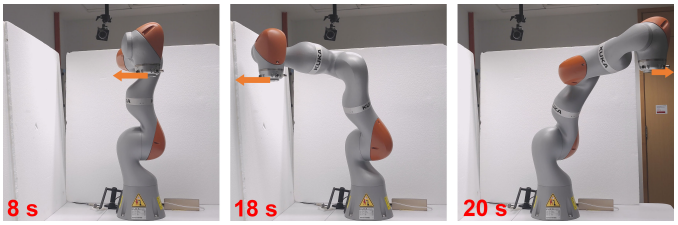

Fig. 3: Snapshots of Test-1, illustrating instability issues under variable impedance control without passivity guarantees. The orange arrows indicate motions of the robot.

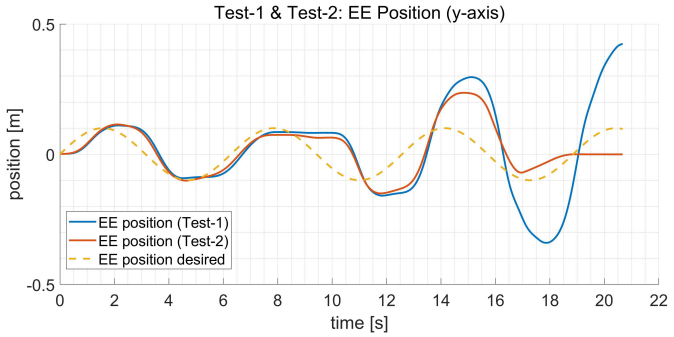

Fig. 4: Comparison of EE's positions for Test-1 and Test-2, where gradual divergence is observed in Test-1, while the robot regains stability in Test-2 by incorporating an energy tank to enforce passivity.

following a reference trajectory with $\dot{x}_{\mathrm{d}} = 0, \ddot{x}_{\mathrm{d}} = 0$ to trigger the recharging operation, and resumes normal operation once the tank is refilled. This experiment is specifically designed to induce instability through continuously varying reference motions and stiffness parameters, and consequently, perfect tracking is inherently unattainable.

For comparison, Test-4 demonstrates that intuitive recharging operations (e.g., recharging once tank depletion) can lead to divergent behaviors similar to Test-1, confirming that arbitrary recharging operations would undermine the passivity guarantees provided by energy tanks. It also highlights the significance of the proposed almost-everywhere-passive condition for safe recharging. Furthermore, Test-5 shows that simply assigning a large initial energy budget can also lead to system instability, emphasizing the practical importance of dynamic recharging approaches for energy tank techniques.

B. Evaluation of Integrated Framework for Safety

To evaluate our integrated safety framework's effectiveness in realistic manipulation scenarios, the robot is then deployed to perform a pick-and-place task. As illustrated in Fig. 1(b), it requires the robot to sequentially grasp 3D-printed cubes and place them at predefined locations while responding to various safety challenges typically encountered in human-robot collaborative environments. Multiple safety-critical scenarios were deliberately introduced during task execution, as shown in Fig. 1(b)-(d). These included both static and dynamic obstacles in proximity to the robot, some detected via motion capture systems (with attached reflective markers) and

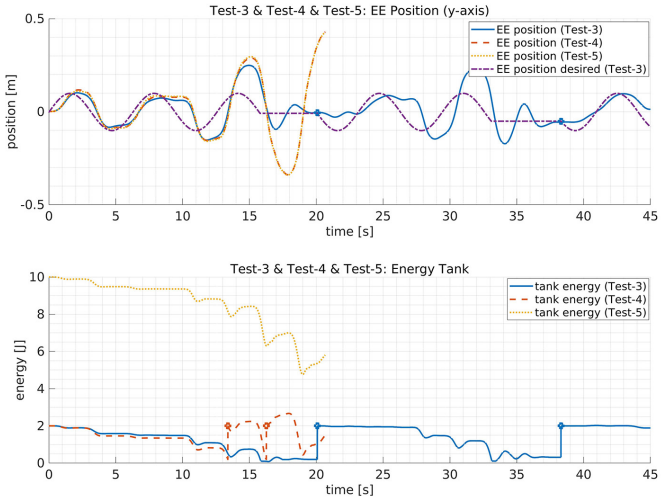

Fig. 5: Results of Test-3, Test-4 and Test-5. Upper: Comparison of EE's positions. Bottom: The level of energy stored in tanks. The circle markers indicate instances of tank recharging events.

TABLE I: Parameter Table

Parameter	Value	Parameter	Value
β_p	1	$\boldsymbol{v}_{\mathrm{up}}$	$[0.3, 0.3, 0.3]$ m/s
β_v	1×10^3	$\boldsymbol{v}_{\mathrm{low}}$	$-\boldsymbol{v}_{\mathrm{up}}$
β_a	3×10^5	$\boldsymbol{a}_{\mathrm{up}}$	$[1.0, 1.0, 1.0]$ m/s^2
T_{init}	5.0 J	$\boldsymbol{a}_{\mathrm{low}}$	$-\boldsymbol{a}_{\mathrm{up}}$
r_i	0.25 m	$\bar{v}_{\mathrm{up}}$	0.3 m/s
P_{limit}	1.0 W	$\bar{v}_{\mathrm{low}}$	0.01 m/s

others intentionally left undetected to evaluate the framework's robustness.

Specifically, the experiments incorporate safety challenges as follows: 1) Avoidance of a static obstacle occupying a placement zone; 2) Avoidance of a dynamic obstacle suddenly intervening in the robot's path; 3) Response to a fast-moving obstacle that causes CBF-QP infeasibility; 4) Adaptation to collision with a fast-moving obstacle; 5) Adaptation to direct human interaction; 6) Adaptation to collision with an undetected obstacle; and 7) Adaptation to collision with a human hand during cube placement. The experimental results demonstrate how the proposed framework addresses these challenges through its integrated, complementary safety paradigms. To be brief, the CBF-QP motion planner generates active collision avoidance for obstacles in cases 1 and 2, while the fallback action tries to maintain safe separation from the obstacle in case 3. For unavoidable collisions (case 4) and unpredicted interactions (case 5-7), the passive safety module is activated to mitigate post-contact impacts. Due to page limit, we refer readers to the supplementary video for comprehensive experimental demonstrations with data visualizations.

For the following tests, the Cartesian stiffness and damping matrices are set to $\boldsymbol{K}_{\mathrm{d}} = \mathrm{diag}(1600\boldsymbol{I}_3, 50\boldsymbol{I}_3)$ and $\boldsymbol{D}_{\mathrm{d}} = \mathrm{diag}(80\boldsymbol{I}_3, 10\boldsymbol{I}_3)$, respectively. Other parameters are listed in Table I.

C. Ablation Study

To evaluate the contribution of each module in our framework, the following ablation tests are conducted

- **Ablation-1**: Active safety module disabled;
- **Ablation-2**: Passive safety module disabled;
- **Ablation-3**: Tank recharging operations disabled.

In each ablation test, the robot performs the same pick-and-place task as in Section IV.B. The results using the complete control framework shown in Section IV.B is referred to as **Ours** for later comparative analysis.

In Ablation-1 (Fig. 6), the robot suffers from collision with both static and dynamic obstacles due to the absence of active avoidance capabilities. Although the passive safety module could maintain collision impacts within bounded ranges, lacking active safety paradigm does compromise the robot's response to diverse safety challenges.

Ablation-2 (Fig. 7) highlights the significance of post-impact mitigation in the presence of humans and obstacles. While passive safety is disabled, the robot is unaware of potential collisions and maintains high stiffness even in contact with humans and other objects. Fig. 8 compares the energy variance and actuation torques between Ablation-2 and Ours, revealing that lacking passive safety results in much higher power exchanges and interaction forces, thus presenting potential risks to both humans (and other objects) and the robot itself. Particularly, the robot collides with a wooden block at 138 s in Ours and at 56 s in Ablation-2 (the right of Fig. 7). Detailed comparison reveals that the passive safety mechanism in Ours activates approximately 0.2 s after initial contact, reducing peak torques to approximately 30% of those in Ablation-2.

Fig. 9 displays the energy tank level in Ablation-3 compared to Ours. The task is terminated in Ablation-3 upon tank depletion, whereas Ours enables continuous execution of the pick-and-place task for approximately three minutes, with multiple recharging operations occurring during operation. Notably, the intervals between the recharging events are different due to dynamic energy exchanges induced by collision avoidance and human interaction. It highlights the adaptive nature of the proposed recharging condition (22), which relies on actual system states rather than predetermined task segmentation.

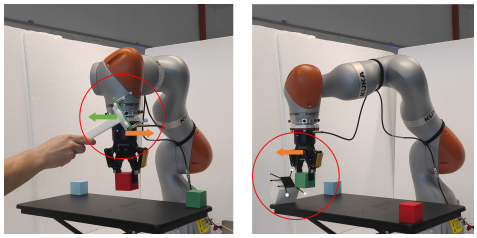

Fig. 6: Snapshots of Ablation-1 (active safety disabled) where the robot loses capability of active avoidance of obstacles. The orange arrows indicate motion directions of the robot, while the green arrow indicates motion direction of the moving obstacle. Left: The robot fails to avoid a moving obstacle that interrupts its path. Right: The robot collides with a static obstacle occupying placement zone.

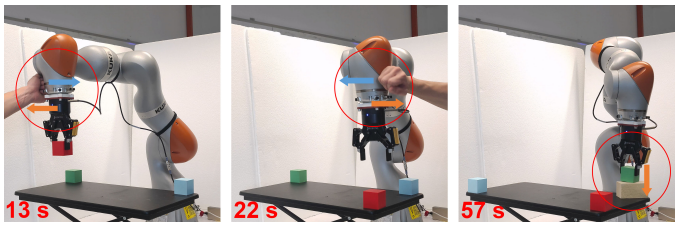

Fig. 7: Snapshots of Ablation-2 (passive safety disabled) where the robot suffers from unexpected collisions. The orange arrows indicate motions of the robot while the blue arrows indicate motions of the human's hand. Left and Center: The robot maintains high stiffness during collision with a human's hand without reactive responses. Right: The robot pushes heavily against a wooden block upon contact.

V. Conclusion

This paper presented a novel control framework that systematically integrates active and passive safety paradigms to address diverse safety challenges for complex interaction tasks in human-shared spaces. It also incorporates an energy tank and a novel tank recharging condition to offer passivity guarantees for tasks with dynamic energy demands. Comprehensive experiments using a KUKA iiwa 14 robot validated the framework's effectiveness and strong robustness. Comparative trials demonstrated the necessity of enforcing passivity for robots under variable impedance control and showed that the proposed tank recharging strategy preserves system passivity while adapting to real-time energy demands without task-specific tuning. Through a pick-and-place manipulation task, the proposed system demonstrated the robot's capability to successfully respond to various safety challenges, such as obstacle avoidance scenarios, direct human interaction, and unexpected collisions. Moreover, ablation studies confirm the contributions of each module to the overall performance.

References

[1] A. D. Ames, X. Xu, J. W. Grizzle, and P. Tabuada, "Control barrier function based quadratic programs for safety critical systems," *IEEE Transactions on Automatic Control*, vol. 62, pp. 3861–3876, 2016.

[2] A. D. Ames, S. Coogan, M. Egerstedt, G. Notomista, K. Sreenath, and P. Tabuada, "Control barrier functions: Theory and applications," in *European control conference (ECC)*, 2019, pp. 3420–3431.

[3] J. Lee, J. Kim, and A. D. Ames, "Hierarchical relaxation of safety-critical controllers: Mitigating contradictory safety conditions with application to quadruped robots," in *2023 IEEE/RSJ International Conference on Intelligent Robots and Systems (IROS)*. IEEE, 2023, pp. 2384–2391.

[4] Z. Jian, Z. Yan, X. Lei, Z. Lu, B. Lan, X. Wang, and B. Liang, "Dynamic control barrier function-based model predictive control to safety-critical obstacle-avoidance of mobile robot," in *2023 IEEE International Conference on Robotics and Automation (ICRA)*, 2023, pp. 3679–3685.

[5] K. Shi and G. Hu, "Dual-mode human-robot collaboration with guaranteed safety using time-varying zeroing control barrier functions and quadratic program," *IEEE Robotics and Automation Letters*, vol. 8, pp. 5902–5909, 2023.

[6] W. S. Cortez, C. K. Verginis, and D. V. Dimarogonas, "Safe, passive control for mechanical systems with application to physical human-robot interactions," in *2021 IEEE International Conference on Robotics and Automation (ICRA)*. IEEE, 2021, pp. 3836–3842.

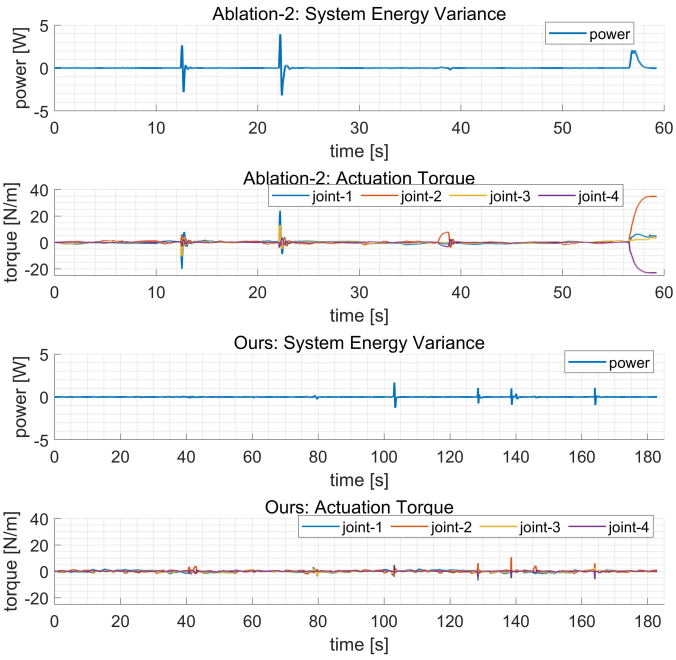

Fig. 8: Comparison between Ablation-2 (passive safety disabled) and Ours, regarding the robot's energy variance and the actuation torques. The three spikes in the top first figure correspond to the three collisions illustrated in Fig. 7.

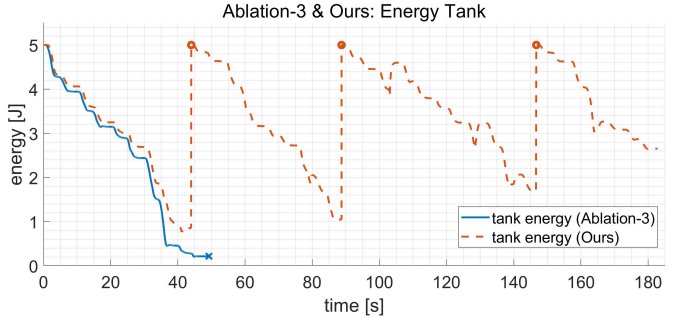

Fig. 9: Comparison between Ablation-3 (recharging disabled) and Ours regarding energy tank level. The cross marker indicates task termination, while the circle markers indicate tank recharging events.

[7] V. N. Sankaranarayanan, A. Saradagi, S. Satpute, and G. Nikolakopoulos, "Time-varying control barrier function for safe and precise landing of a uav on a moving target," in *2024 IEEE/RSJ International Conference on Intelligent Robots and Systems (IROS)*, 2024, pp. 8075–8080.

[8] S. Stramigioli, "Energy-aware robotics," in *Mathematical control theory I: Nonlinear and hybrid control systems*. Springer, 2015, pp. 37–50.

[9] F. Ferraguti, C. Secchi, and C. Fantuzzi, "A tank-based approach to impedance control with variable stiffness," in *2013 IEEE International Conference on Robotics and Automation (ICRA)*, 2013, pp. 4948–4953.

[10] Y. Michel, M. Saveriano, and D. Lee, "A novel safety-aware energy tank formulation based on control barrier functions," *IEEE Robotics and Automation Letters*, 2024.

[11] E. Shahriari, L. Johannsmeier, and S. Haddadin, "Valve-based virtual energy tanks: A framework to simultaneously passify controls and embed control objectives," in *2018 Annual American Control Conference (ACC)*. IEEE, 2018, pp. 3634–3641.

[12] K. Karacan, H. Sadeghian, R. Kirschner, and S. Haddadin, "Passivity-based skill motion learning in stiffness-adaptive unified force-impedance control," in *2022 IEEE/RSJ International Conference on Intelligent Robots and Systems (IROS)*. IEEE, 2022, pp. 9604–9611.

[13] S. Hjorth, E. Lamon, D. Chrysostomou, and A. Ajoudani, "Design of an energy-aware cartesian impedance controller for collaborative disassembly," in *2023 IEEE International Conference on Robotics and Automation (ICRA)*. IEEE, 2023, pp. 7483–7489.

[14] R. Rashad, D. Bicego, J. Zult, S. Sanchez-Escalonilla, R. Jiao, A. Franchi, and S. Stramigioli, "Energy aware impedance control of a flying end-effector in the port-hamiltonian framework," *IEEE Transactions on Robotics*, vol. 38, pp. 3936–3955, 2022.

[15] D. Lee and K. Huang, "Passive-set-position-modulation framework for interactive robotic systems," *IEEE Transactions on Robotics*, vol. 26, pp. 354–369, 2010.

[16] B. Gerlagh, F. Califano, S. Stramigioli, and W. Roozing, "Energy-aware adaptive impedance control using offline task-based optimization," in *2021 20th International Conference on Advanced Robotics (ICAR)*. IEEE, 2021, pp. 187–194.

[17] F. Califano, D. van Dijk, and W. Roozing, "A task-based post-impact safety protocol based on energy tanks," *IEEE Robotics and Automation Letters*, vol. 7, pp. 8791–8798, 2022.

[18] D. Sacerdoti, F. Benzi, and C. Secchi, "A reinforcement learning-based control strategy for robust interaction of robotic systems with uncertain environments," in *2024 IEEE International Conference on Robotics and Automation (ICRA)*, 2024, pp. 5788–5794.

[19] F. Califano, R. Rashad, C. Secchi, and S. Stramigioli, "On the use of energy tanks for robotic systems," in *International Workshop on Human-Friendly Robotics*, 2022, pp. 174–188.

[20] F. Benzi and C. Secchi, "An optimization approach for a robust and flexible control in collaborative applications," in *2021 IEEE International Conference on Robotics and Automation (ICRA)*, 2021, pp. 3575–3581.

[21] Z. Zhang, T. Li, and N. Figueroa, "Constrained passive interaction control: Leveraging passivity and safety for robot manipulators," in *2024 IEEE International Conference on Robotics and Automation (ICRA)*, 2024, pp. 13 418–13 424.

[22] B. Siciliano, L. Sciavicco, L. Villani, and G. Oriolo, "Robotics: Modelling, planning and control," *Advanced Textbooks in Control and Signal Processing*, 2009.

[23] C. Ott, *Cartesian impedance control of redundant and flexible-joint robots*. Springer, 2008.

[24] N. Hogan, "Impedance control: An approach to manipulation, part ii—implementation," *ASME Journal of Dynamic Systems, Measurement, and Control*, vol. 107, pp. 8–16, 1985.

[25] E. Cuniato, N. Lawrance, M. Tognon, and R. Siegwart, "Power-based safety layer for aerial vehicles in physical interaction using lyapunov exponents," *IEEE Robotics and Automation Letters*, vol. 7, no. 3, pp. 6774–6781, 2022.

[26] A. Van Der Schaft, "Port-hamiltonian systems: an introductory survey," in *Proceedings of the international congress of mathematicians*, vol. 3, 2006, pp. 1339–1365.

[27] F. Ferraguti, M. Bertuletti, C. T. Landi, M. Bonfè, C. Fantuzzi, and C. Secchi, "A control barrier function approach for maximizing performance while fulfilling to iso/ts 15066 regulations," *IEEE Robotics and Automation Letters*, vol. 5, no. 4, pp. 5921–5928, 2020.

[28] ISO/TS 15066:2016, "Robots and robotic devices – collaborative robots," [Online]. Available: https://www.iso.org/standard/62996.html.

[29] K. Chatzilygeroudis, M. Mayr, B. Fichera, and A. Billard, "iiwa_ros: A ros stack for kuka's iiwa robots using the fast research interface," 2019. [Online]. Available: http://github.com/epfl-lasa/iiwa_ros